The Astrophysical Journal, 640:530–537, 2006 March 20

SPECTRAL SUBTRACTION: A NEW APPROACH TO REMOVE LOW- AND HIGH-ORDER SPECKLE NOISE

Deqing Ren and Haimin Wang
Department of Physics, New Jersey Institute of Technology, Newark, NJ 07102
Received 2005 September 15; accepted 2005 November 18

ABSTRACT

We present a novel "spectral subtraction algorithm" (SSA) technique to remove speckle noise. It consists of a low-order and a high-order SSA and is based on a three-dimensional image spectroscopy in which the three-dimensional data cube is available and thus the speckle noise introduced by the wave-front error can be efficiently subtracted. For the low-order SSA, speckles up to the second or third order can be totally subtracted, leaving the residual speckles dominated only by the third or fourth order, respectively, and imaging contrast is increased consequently; for the high-order SSA, speckles up to the fourth or fifth order can be subtracted, leaving the residual speckles dominated only by the fifth or sixth order, respectively, and the performance is further improved. This is the first demonstration that such high-order speckles could be subtracted. Since the SSAs are conducted over a wide spectral band, a *white-light image* can be re-assembled from the three-dimensional data cube. The white-light image would increase the single-to-noise ratio and reduce the exposure time, which are crucial for the search of faint companion objects. Combined with a coronagraph, the SSA can provide an extra contrast gain for the coronagraph imaging, relax the requirement for the wave-front quality (no adaptive optics correction is required for a space-borne imaging system), and significantly increase the performance of exoplanet imaging and biomarker spectroscopy.

Subject headings: instrumentation: miscellaneous — planetary systems — techniques: high angular resolution — techniques: image processing

Online material: color figures

1. INTRODUCTION

To discover life on another planet is potentially one of the most important scientific advances of this century. Advances in the past decade using indirect imaging methods, such as measuring the "wobble" of planet-star systems (Marcy et al. 2002; Butler et al. 2003; Tinney et al. 2003), infer that exoplanets might be common. The search for habitability and for life requires that we can detect photons directly from planets and use spectroscopy to analyze physical and atmospheric conditions. Such detection remains technologically very challenging, since very high contrast ratio and small angular separation are involved.

Recently, coronagraphs for high-contrast imaging were proposed for the exoplanet detection (Ren & Serabyn 2005; Vanderbei et al. 2005; Guyon et al. 2005; Kasdin et al. 2003; Gonsalves & Nisenson 2003; Kuchner & Traub 2002; Nisenson & Papaliolios 2001; Rouan et al. 2000; Baudoz et al. 2000). A 10^{-10} contrast at $4\lambda/D$ in the visible is required for NASA's *TPF-C* (*Terrestrial Planet Finder–Coronagraph*) space mission. Although in the perfect case these coronagraphs may provide a contrast better than 10^{-10} theoretically, the actual performance for a coronagraph is dominated by the speckle noise introduced by the wave-front error (Kasdin et al. 2004). Therefore, it is very difficult to deliver the required performance. The speckle fluctuates with a dwell time of several seconds for a space telescope, making it difficult to remove or average out. Furthermore, the size of the speckle is very similar to that of the companion's image and is a potential source of false signal. To overcome these difficulties, many pioneer researches have been conducted in recent years (Bloemhof 2003, 2004a, 2004b; Bloemhof & Oppenheimer 2001; Aime & Soummer 2004; Perrin et al. 2003; Boccatletti et al. 2002; Sivaramakrishnan et al. 2001, 2002; Sparks & Ford 2002; Marois et al. 2000; Racine et al. 1999), which greatly improved the understanding of speckle properties.

In general, the wave-front error can be expressed as a Taylor series, in which the low-order speckles are the dominant noise. Unfortunately, previous work of image rotation and subtraction only allows one of the low-order terms to be eliminated, leaving the speckle noise still dominated by one of the residual low-order terms that is either the linear or the quadratic term. In this paper, we propose a low-order and a high-order spectral subtraction algorithm (SSA) that could completely remove the low-order (both the linear and the quadratic terms) and the high-order speckles, respectively, so that the overall speckle noise could be significantly reduced, making the residual speckles dominated only by other higher order speckles. This approach is based on a three-dimensional image spectroscopy that can be realized by an integral field unit (IFU) (Ren & Ge 2004; Ren & Allington-Smith 2002) in which the three-dimensional data cube (x, y, and λ) can be collected simultaneously. Thus, it eliminates any possible system error in getting the three-dimensional data cube as by the conventional long-slit spectrograph. The three-dimensional imaging is also a natural choice for the spectroscopy of the biomarkers via simultaneously sampling two-dimensional star disk for spectroscopy, where the exoplanets may be located.

Although there are some approaches based on the wavelength and intensity scaling (Sparks & Ford 2002; Racine et al. 1999), their performance is limited when wave-front errors are present. The spectral deconvolution (Sparks & Ford 2002) is suitable for middle- or high-frequency wave-front error where the wave-front error introduced by the mirror surface roughness is extremely small ($\sim$0.999 Strehl ratio). The direct two-wavelength subtraction (Racine et al. 1999) is limited by the residual speckles, which are a function of the wave-front error. Marois et al. (2000) proposed an improved approach based on a three-wavelength subtraction, and it is not clear whether such an approach could remove all the low-order speckles. We demonstrate that based on a direct subtraction of the "image rotation and subtraction," the SSAs proposed herein can simultaneously eliminate not only the low-order, but also the high-order speckles. Our SSAs are a further extension of the differential imaging

(Racine et al. 1999; Rosenthal et al. 1996) and could be used with a coronagraph to further improve the actual performance when a moderate wave-front error is present. Although a circular aperture is used to derive the algorithms, the results are valid for any coronagraph with a symmetrical aperture that has an even pupil function, such as nulling (Ren & Serabyn 2005; Baudoz et al. 2000), shaped-pupil (Vanderbei et al. 2005; Kasdin et al. 2003), band-limited (Kuchner & Traub 2002), and apodized pupil (Nisenson & Papaliolios 2001) coronagraphs, which are almost all the available coronagraphs with high-contrast imaging ability.

A coronagraph removes most of the unaberrated starlight. Because of the wave-front error, which is inherent in any optical system (and atmospheric turbulence for ground observing), the coronagraph cannot deliver its theoretical performance. In such a case, a three-dimensional imaging spectrograph located at the coronagraph's focal plane could be used to provide an extra gain for the high contrast imaging as well as for spectroscopy by simultaneously sampling the two-dimensional star disk. The idea that a three-dimensional based spectroscopy coupled with a coronagraph could be used to remove the scattered light and thus provide a contrast gain was first proposed by Sparks & Ford (2002). We have noted that *TPF-C* may provide resolving power $\sim$100 for spectroscopy. As we show below, the SSA that we propose could provide a significant contrast gain at this resolving power. For a space telescope and imaging system, wave-front errors may be introduced by mirror surface figure errors, telescope distortion caused by rotation, and optical alignment errors. Since such wave-front errors are expected to be in low frequencies, we only use the low-frequency wave-front errors as an example to demonstrate the performance of the SSAs. This does not diminish the generality that they should also be suitable for the middle- or high-frequency wave-front error.

In § 2, we present the general speckle modeling, which serves as a fundamental mathematical tool to describe the speckle noise. Details of the low- and high-order SSAs are discussed in § 3. PSF centering sensitivity is discussed in § 4. Conclusions are presented in § 5. Since the speckle is the dominant noise, other types of noise, such as detector and photon statistic noises, are not discussed in detail in this article.

2. SPECKLE MODELING

It is well known that the aberrated PSF of a monochromatic wavelength at the focal plane can be expressed as the square modulus of a Fourier transform of the pupil function and the wave-front error Φ:

$$I(r,\ \lambda) = \left|\overline{(Ae^{i\Phi})}\right|^2, \tag{1}$$

where A is the nominal pupil function, which is 1 in the pupil and 0 elsewhere, r is the two-dimensional coordinate vector on the image plane, and λ is the wavelength. The overline denotes the two-dimensional Fourier transform. Assuming that the pupil is symmetric, then A is real and even. This is true for most of the coronagraphs, such as those with circle, square, apodized, and shaped pupils. For small optical aberrations (much less than 1 rad), i.e., at high Strehl ratio, the phase can be expressed as a convergent Taylor series $e^{i\Phi} = 1 + i\Phi - \Phi^2/2 - i\Phi^3/6 + \Phi^4/24 + \ldots$. A full expansion of the speckles for the aberrated PSF was discussed by Perrin et al. (2003). Here we rederive it according to our application in different format up to the fourth-order speckle. Since Φ is defined in the pupil, one has $A\Phi = \Phi$. The focal plane intensity distribution up to the fourth-order speckle can be expressed as

$$\begin{aligned} I(r,\ \lambda) = {} & \left|\bar{A}\right|^2 - i\left[\bar{A}\bar{\Phi}^* - \bar{A}^*\bar{\Phi}\right] + \left|\bar{\Phi}\right|^2 \\ & - \left[\bar{A}\left(\bar{\Phi}^* \otimes \bar{\Phi}^*\right) + \bar{A}^*\left(\bar{\Phi} \otimes \bar{\Phi}\right)\right]/2 \\ & - i\left[\bar{\Phi}\left(\bar{\Phi}^* \otimes \bar{\Phi}^*\right) - \bar{\Phi}^*\left(\bar{\Phi} \otimes \bar{\Phi}\right)\right]/2 \\ & + i\left[\bar{A}\left(\bar{\Phi}^* \otimes \bar{\Phi}^* \otimes \bar{\Phi}^*\right) - \bar{A}^*\left(\bar{\Phi} \otimes \bar{\Phi} \otimes \bar{\Phi}\right)\right]/6 \\ & + \left[\bar{A}\left(\bar{\Phi}^* \otimes \bar{\Phi}^* \otimes \bar{\Phi}^* \otimes \bar{\Phi}^*\right) + \bar{A}^*\left(\bar{\Phi} \otimes \bar{\Phi} \otimes \bar{\Phi} \otimes \bar{\Phi}\right)\right]/24 \\ & - \left[\bar{\Phi}\left(\bar{\Phi}^* \otimes \bar{\Phi}^* \otimes \bar{\Phi}^*\right) + \bar{\Phi}^*\left(\bar{\Phi} \otimes \bar{\Phi} \otimes \bar{\Phi}\right)\right]/6 \\ & + \left|\bar{A} \otimes \bar{\Phi} \otimes \bar{\Phi}\right|^2/4, \end{aligned} \tag{2}$$

where $\otimes$ and * denote the convolution and complex conjugate operation, respectively. The above equation can be further simplified as

$$I(r,\ \lambda) = \left|\bar{A}\right|^2 + I_{\text{even2}} + I_{\text{even4}} + I_{\text{odd1}} + I_{\text{odd3}}, \tag{3}$$

where

$$I_{\text{even2}} = \left|\bar{\Phi}\right|^2 - \text{Re}\left[\bar{A}(\bar{\Phi}^* \otimes \bar{\Phi}^*)\right],$$

$$\begin{aligned} I_{\text{even4}} = {} & \text{Re}\left[\bar{A}\left(\bar{\Phi}^* \otimes \bar{\Phi}^* \otimes \bar{\Phi}^* \otimes \bar{\Phi}^*\right)\right]/12 \\ & - \text{Re}\left[\bar{\Phi}\left(\bar{\Phi}^* \otimes \bar{\Phi}^* \otimes \bar{\Phi}^*\right)\right]/3 + \left|\bar{\Phi} \otimes \bar{\Phi}\right|^2/4, \end{aligned}$$

$$I_{\text{odd1}} = 2\text{Im}\left[\bar{A}\bar{\Phi}^*\right], \text{ and}$$

$$I_{\text{odd3}} = \text{Im}\left[\bar{\Phi}\left(\bar{\Phi}^* \otimes \bar{\Phi}^*\right)\right] - \text{Im}\left[\bar{A}\left(\bar{\Phi}^* \otimes \bar{\Phi}^* \otimes \bar{\Phi}^*\right)\right]/3,$$

where Im and Re denote the imaginary and real parts, respectively. Since A and Φ are real, the corresponding Fourier transforms $\bar{A}$ and $\bar{\Phi}$ will be Hermitian functions (Bracewell 1986). $\bar{A}$ will also be real and even, and Φ is not necessarily even. Therefore, the terms $|\bar{A}|^2$, I_{even2}, and I_{even4} are even; the terms I_{odd1} and I_{odd3} are odd. The speckle noise, which is a real function, can be eventually expressed as a combination of the even and odd terms. This is not surprising, since any real function can be expressed as an addition of an even and an odd function.

In equation (2), the first term $|\bar{A}|^2$ is the perfect PSF without wave-front errors, and the remaining terms are speckle noise. $\bar{\Phi}$ and $\bar{\Phi}^*$ have the same modulus and only have a different phase. They have a similar contribution to the intensity of the speckle noise and are therefore called first-order speckle. Similarly, $|\bar{\Phi}|^2$ and $(\bar{\Phi}^* \otimes \bar{\Phi}^*)$ are called second-order speckle. Such a definition is also suitable for higher order speckles. Therefore, the terms I_{odd1}, I_{even2}, I_{odd3}, and I_{even4} are called first-order, second-order, third-order, and fourth-order speckle noise, respectively. The modulus of the second-order speckle is equal to the square of the modulus of the first-order speckle. As a result, the second-order speckle will be less than the first-order in amplitude. Obviously, a high-order speckle noise will have a smaller amplitude than that of a low-order noise.

The intensity distribution of the speckle noise is a function of the wave-front error on the pupil. For a high-frequency component of the wave-front error, the first-order speckle $\bar{\Phi}$ (or $\bar{\Phi}^*$) will of course correspond to a high-frequency spectrum that is located far away from the PSF on the focal plane. Therefore, a low-frequency wave-front error tends to induce a speckle noise closely around the PSF, while a high-frequency error tends to introduce a speckle noise distributed over a large area. The actual

intensity distribution for the different order speckle noise is somewhat complicated since it may involve a modulation with the perfect PSF and a convolution as shown in equation (2), which may result in a more complicated speckle distribution. But the conclusion derived from the first-order speckle is generally true, which will be further confirmed by our simulations in § 3.

If $e^{i\Phi} = 1 + i\Phi$, equation (3) becomes

$$I(r,\ \lambda) = \left|\bar{A}\right|^2 + 2\mathrm{Im}\left[\bar{A}\left(\bar{A}^* \otimes \bar{\Phi}^*\right)\right] + \left|\bar{A} \otimes \bar{\Phi}\right|^2.$$

The low-order terms $2\mathrm{Im}[\bar{A}(\bar{A}^* \otimes \bar{\Phi}^*)]$ and $|\bar{A} \otimes \bar{\Phi}|^2$ are the dominant speckle noise, in which the $2\mathrm{Im}[\bar{A}(\bar{A}^* \otimes \bar{\Phi}^*)]$ is larger than the $|\bar{A} \otimes \bar{\Phi}|^2$ term at high Strehl ratio. The $2\mathrm{Im}[\bar{A}(\bar{A}^* \otimes \bar{\Phi}^*)]$ term is called the linear term, while $|\bar{A} \otimes \bar{\Phi}|^2$ is called the quadratic term (Bloemhof 2004b). If both the low-order terms were simultaneously eliminated, leaving the residual speckle noise determined only by high-order terms, the speckle noise would be dramatically reduced. In equation (3), the remaining terms, which do not include the two low-order terms of $2\mathrm{Im}[\bar{A}(\bar{A}^* \otimes \bar{\Phi}^*)]$ and $|\bar{A} \otimes \bar{\Phi}|^2$, are called high-order speckles.

The odd terms I_{odd1} and I_{odd3} have negative and positive values and a zero mean. Therefore, in principle, they could be averaged out to zero by a long exposure. However, such an averaging out has not yet been demonstrated in practice. Although the even terms I_{even2} and I_{even4} contribute a positive intensity, which may reduce the dynamic range for the high-contrast imaging, they are smaller in amplitude than the corresponding even terms I_{odd1} and I_{odd3} and could be efficiently subtracted, as we demonstrate in the following sections.

The fact that the speckle noise could be decomposed as different orders in respect to $\bar{\Phi}$ provides an opportunity to remove the speckles. Since the low-order speckles are the dominant noise, the main goal of the data reduction is to eliminate both the linear and the quadratic terms simultaneously.

2.1. *Direct Subtraction*

In equation (3), all the even terms can be directly eliminated by subtracting a copy of the original image with a 180° rotation around the PSF center. For such a co-subtracted image, one has

$$I(r,\ \lambda)_{\mathrm{sub}} = I_{\mathrm{odd1}} + I_{\mathrm{odd3}}. \tag{4}$$

Since the starlight intensity for the odd terms will be doubled after the co-subtraction, $I(\lambda)_{\mathrm{sub}}$ is the intensity distribution of the co-subtracted image divided by 2. In the above equation, the perfect PSF $|\bar{A}|^2$ is also subtracted because of its symmetry. The subtraction will create two identical companion's images, one is positive while the other is negative.

Similar, all the odd terms in equation (3) can be directly eliminated by adding a copy of the original image with a 180° rotation around the PSF center. For such a co-added image, one has

$$I(r,\ \lambda)_{\mathrm{add}} = I_{\mathrm{even2}} + I_{\mathrm{even4}}. \tag{5}$$

Again since the starlight intensity for the even terms will be doubled after the co-addition, $I(\lambda)_{\mathrm{add}}$ is the intensity distribution of the co-added image divided by 2. Because of the image rotation, the co-added image will contain two identical positive planet images. Note that the perfect PSF is not included in the above equation, although it could not be eliminated via such an addition. However, the perfect PSF can be reconstructed and then subtracted once one knows the wavelength and peak intensity. This information is available in the three-dimensional data cube. Also note that for a high-contrast coronagraph, such as the shaped pupil (Kasdin et al. 2003), it is not necessary to remove the perfect PSF, since we are only interested in the discovery area that is typically located $(4\text{–}10)\lambda/D$ away from the PSF center and where a high-contrast image 10^{-10} is available for such a perfect PSF (assume that the detectors are antibloom).

The direct subtraction (i.e., image rotation and subtraction) was used to analyze the speckle properties of the linear term $2\mathrm{Im}[\bar{A}(\bar{A}^* \otimes \bar{\Phi}^*)]$ and the quadratic term $|\bar{A} \otimes \bar{\Phi}|^2$ (Bloemhof 2004b; Perrin et al. 2003). But such an approach cannot remove both the linear and quadratic terms simultaneously. To improve the contrast performance, a further step that can remove both the low-order speckle terms is needed.

Although the linear or quadratic term can also be eliminated by using the low-order SSA, which is discussed in the next section, the low-order SSA can only subtract one order of speckle after each operation. The direction subtraction expressed by equations (4) and (5), however, can eliminate all the low- and high-order even or odd terms, respectively, and is also straightforward and simple to implement.

Both equations (4) and (5) are valid for any symmetrical aperture and are called direct subtraction herein. It is in fact a process to isolate the even and the odd speckle terms. Such an isolation is necessary for further data reduction to eliminate speckles of the specific orders, as is discussed in the next section.

3. SPECTRAL SUBTRACTION

Assume that the intensity $I(r, \lambda)$ at different wavelengths can be calibrated so that the intensity is identical at different wavelengths. Although such an assumption is not necessary for the spectral subtraction, it can simplify the expression. For an imaging system, the wave-front error at the pupil can be expressed as

$$\Phi(\lambda) = \frac{2\pi\Delta S}{\lambda}, \tag{6}$$

where Φ is in radians and ΔS is the optical path error, which is a constant during each speckle dwell life time and is independent of the wavelength. This is true for a space imaging system that deploys only mirrors. The relationship between the wave-front errors at two different wavelengths can be expressed as $\Phi_2 = \Phi_1\lambda_1/\lambda_2$. For the corresponding Fourier transform, one has

$$\bar{\Phi}_2 = \frac{\lambda_1}{\lambda_2}\bar{\Phi}_1, \quad \bar{\Phi}_2^* = \frac{\lambda_1}{\lambda_2}\bar{\Phi}_1^*. \tag{7}$$

From equations (4) and (5), it is evident that the speckles are modulated by the aperture function $\bar{A}$, which in turn is a function of wavelength (note that $\Phi = A\Phi$). Speckles at different wavelengths can be scaled to the same wavelength and then the specific order can be subtracted to zero: one of the PSFs needs to be scaled according to the wavelength so that the subtraction is done at the same wavelength. Assume that the absorption spectral image and the continuum spectral image are at wavelengths λ_i and $\lambda_i + \Delta\lambda$, respectively. By proper intensity scaling, the specific speckle term can be eliminated

$$\begin{aligned}\Delta I &= I_i(r,\ \lambda_i) - kI_i(r,\ \lambda_i + \Delta\lambda)\\ &= 0 \quad \text{for specific term},\end{aligned} \tag{8}$$

where ΔI is the residual speckle noise, k is an intensity scale factor that ensures that the specific speckle term can be totally

subtracted, and ΔI is a function of the wavelength λ_i and $\Delta\lambda$. As we will see in an example, k is very close to 1. Here $I_i(r, \lambda_i)$ is the absorption spectral image at the absorption wavelength λ_i. Since the wavelengths are different for the absorption image $I_i(r, \lambda_i)$ and the continuum image $I_{i+\Delta\lambda}(r,\ \lambda_i + \Delta\lambda)$, the image $I_{i+\Delta\lambda}(r,\ \lambda_i + \Delta\lambda)$ needs to be scaled to wavelength λ_i from the PSF $I_{i+\Delta\lambda}(r,\ \lambda_i + \Delta\lambda)$ at wavelength $\lambda_i + \Delta\lambda$. The wavelength scaled image is expressed as $I_i(r,\ \lambda_i + \Delta\lambda)$ and this results in a monochromatic image at λ_i. For the subtraction, the wave-front error is also scaled to Φ which is the wave-front error at the wavelength λ_i, and the scaling is conducted according to equation (7), where $\Delta\lambda$ is the wavelength difference between the two images to be subtracted.

3.1. *Low-Order SSA*

3.1.1. *Second-Order SSA*

If the first-order term I_{odd1} in equation (4) is eliminated, the residual speckles would be dominated by the third-order term I_{odd3}, which is much smaller than I_{odd1}. Using equation (8), the low-order term I_{odd1} can be eliminated. This is done by setting the term I_{odd1} to be zero, and one has

$$\begin{aligned}\Delta I_i(\lambda_i) &= I_i(r,\ \lambda_i) - kI_i(r,\ \lambda_i + \Delta\lambda)\\ &= \left\{1 - [\lambda_i/(\lambda_i + \Delta\lambda)]^2\right\} I_{\text{odd3}},\end{aligned} \tag{9}$$

where $k = (\lambda_i + \Delta\lambda)/\lambda_i$. The first-order speckle is now totally removed, and the residual speckle noise $\Delta I_i(\lambda_i)$ is only determined by the high-order term I_{odd3}. Furthermore, the term I_{odd3} is reduced by a factor of $1 - [\lambda_i/(\lambda_i + \Delta\lambda)]^2 \approx 2/R$, where $R = \lambda_i/\Delta\lambda$ is the spectral resolution for the subtraction. The residual speckle noise could be linearly reduced by increasing the spectral resolution. Since this approach can remove the speckle noise up to second-order (the second order is removed by the direct subtraction), it is called second-order SSA or simply low-order SSA.

3.1.2. *Third-Order SSA*

Similarly, using equation (8) the second-order term I_{even2} in equation (5) can be eliminated, leaving the noise dominated by the fourth-order speckle. This is done by letting the term I_{even2} be zero, and thus one has

$$\begin{aligned}\Delta I_i(\lambda_i) &= I_i(r,\ \lambda_i) - k\, I_i(r,\ \lambda_i + \Delta\lambda)\\ &= \left\{1 - [\lambda_i/(\lambda_i + \Delta\lambda)]^2\right\} I_{\text{even4}},\end{aligned} \tag{10}$$

where $k = [(\lambda_i + \Delta\lambda)/\lambda_i]^2$. Now, both $|\bar{\Phi}|^2$ and $-\text{Re}[\bar{A}(\bar{A}^* \otimes \bar{\Phi}^* \otimes \bar{\Phi}^*)]$ in the I_{even2} are removed, leaving the residual speckle noise $\Delta I_i(\lambda_i)$ dominated only by the fourth-order term I_{even4}. Again, the term I_{even4} is reduced by a factor of $\sim 2/R$. Since this approach can remove the speckle noise up to the third order (the third order is removed by the direct subtraction), it is called third-order SSA or simply low-order SSA.

3.2. *High-Order SSA*

3.2.1. *Fourth-Order SSA*

The spectral subtractions can also be applied to high-order speckles. Assume that the absorption spectral image is at λ_i and the two continuum spectral images are at wavelengths $\lambda_i - \Delta\lambda$ and $\lambda_i + \Delta\lambda$, respectively. In equation (9) the residual speckles are determined by the I_{odd3} term, which can be eliminated by using the images simultaneously taken at the three wavelengths $\lambda_i - \Delta\lambda$, λ_i, and $\lambda_i + \Delta\lambda$. From equation (9), the residual speckle noise $\Delta\Delta I_i$ that is determined by the speckles higher than the third order is

$$\begin{aligned}\Delta\Delta I_i = &[I_i(\lambda_i + \Delta\lambda) - k_1 I_i(\lambda_i)]\\ &- kk[I_i(\lambda_i) - k_2 I_i(\lambda_i - \Delta\lambda)] = 0\end{aligned} \tag{11}$$

where

$$kk = -\frac{1}{1 - [\lambda_i/(\lambda_i - \Delta\lambda)]^2}\frac{(2\lambda_i + \Delta\lambda)\Delta\lambda\lambda_i}{(\lambda_i + \Delta\lambda)^3},$$

$$I_i(\lambda_i + \Delta\lambda) - k_1 I_i(\lambda_i) = -\left[(2\lambda_i + \Delta\lambda)\Delta\lambda\lambda_i/(\lambda_i + \Delta\lambda)^3\right] I_{\text{odd3}},$$

$$k_1 = \lambda_i/(\lambda_i + \Delta\lambda),$$

$$I_i(\lambda_i) - k_2 I_i(\lambda_i - \Delta\lambda) = \left\{1 - [\lambda_i/(\lambda_i - \Delta\lambda)]^2\right\} I_{\text{odd3}},$$

$$\text{and } k_2 = (\lambda_i - \Delta\lambda)/\lambda_i,$$

where the residual speckle noise $\Delta\Delta I_i$ is zero for the speckles up to the fourth order. Here kk is an intensity scale factor and is close to 1. If we carefully choose the constant kk, the term I_{odd3} can be eliminated, leaving the residual speckle noise $\Delta\Delta I_i$, which is determined by the orders higher than the fourth order. In equation (11), $I_i(\lambda_i + \Delta\lambda) - k_1 I_i(\lambda_i)$ performs the second-order SSA subtraction at wavelengths λ_i and $\lambda_i + \Delta\lambda$, while $I_i(\lambda_i) - k_2 I_i(\lambda_i - \Delta\lambda)$ at wavelengths $\lambda_i - \Delta\lambda$ and λ_i. Both the second-order SSA subtractions result in a residual speckle noise that is determined by the I_{odd3} term, so that by carefully adjusting the intensity scale factor kk, $\Delta\Delta I_i = [I_i(\lambda_i + \Delta\lambda) - k_1 I_i(\lambda_i)] - kk[I_i(\lambda_i) - k_2 I_i(\lambda_i - \Delta\lambda)$ can be zero for the speckles up to the fourth order, and thus its residual noise is dominated by the fifth-order speckle. The constant k_1 and k_2 are close to 1 and can be inferred from equation (9). For the subtraction, all the images are scaled to the wavelength λ_i and the wave-front errors are scaled to Φ, which is the wave-front error at the wavelength λ_i. Equation (11) is called fourth-order SSA or simply high-order SSA.

3.2.2. *Fifth-Order SSA*

Similar, the term I_{even4} in equation (10) can be eliminated by the image subtraction at three wavelengths $\lambda_i - \Delta\lambda$, λ_i, and $\lambda_i + \Delta\lambda$, leaving the residual speckle noise that is determined by the orders higher than the fifth. From equation (10), the residual speckle noise $\Delta\Delta I_i$ becomes

$$\begin{aligned}\Delta\Delta I_i = &[I_i(\lambda_i + \Delta\lambda) - k_1 I_i(\lambda_i)]\\ &- kk[I_i(\lambda_i) - k_2 I_i(\lambda_i - \Delta\lambda)] = 0,\end{aligned} \tag{12}$$

where

$$kk = -\frac{1}{1 - [\lambda_i/(\lambda_i - \Delta\lambda)]^2}\frac{(2\lambda_i + \Delta\lambda)\Delta\lambda\lambda_i^2}{(\lambda_i + \Delta\lambda)^4},$$

$$I_i(\lambda_i + \Delta\lambda) - k_1 I_i(\lambda_i) = -\left[(2\lambda_i + \Delta\lambda)\Delta\lambda\lambda_i^2/(\lambda_i + \Delta\lambda)^4\right] I_{\text{even4}},$$

$$k_1 = [\lambda_i/(\lambda_i + \Delta\lambda)]^2,$$

$$I_i(\lambda_i) - k_2 I_i(\lambda_i - \Delta\lambda) = \left\{1 - [\lambda_i/(\lambda_i - \Delta\lambda)]^2\right\} I_{\text{even4}},$$

$$\text{and } k_2 = [(\lambda_i - \Delta\lambda)/\lambda_i]^2.$$

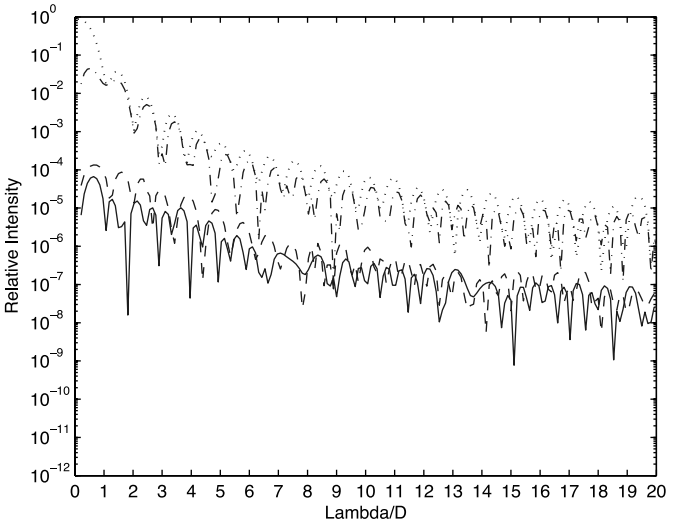

FIG. 1.—Contrast achieved with the low-order SSA at 0.90 Strehl ratio. Dotted line shows the aberrated PSF. Dash-dotted line shows the speckle noise after the perfect star PSF is removed. Solid and dashed lines represent residual speckle noise after the third-order and second-order SSA subtractions, respectively. Contrast gain is typically $\sim 10^{-2}$. [*See the electronic edition of the Journal for a color version of this figure.*]

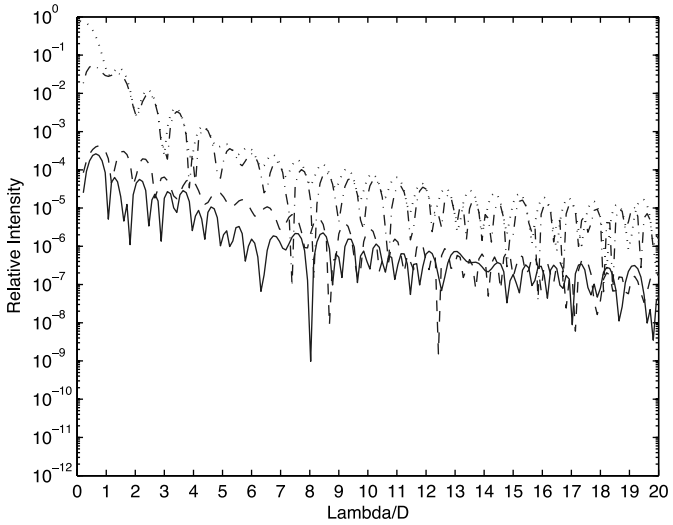

FIG. 2.—Same as Fig. 1, except that the Strehl ratio is 0.80. Contrast gain is typically $\sim 10^{-2}$. [*See the electronic edition of the Journal for a color version of this figure.*]

Evidently, the residual speckle noise $\Delta\Delta I_i$ is zero for the speckles up to fifth order; *kk* is an intensity scale factor and is close to 1. By carefully choosing the constant *kk*, the term $I_{\rm even4}$ can be eliminated, leaving the residual speckle noise $\Delta\Delta I_i$ that is dominated by the sixth order. In equation (12), $I_i(\lambda_i + \Delta\lambda) - k_1 I_i(\lambda_i)$ conducts the third-order SSA subtraction between wavelengths of λ_i and $\lambda_i + \Delta\lambda$, while $I_i(\lambda_i) - k_2 I_i(\lambda_i - \Delta\lambda)$ is between wavelengths of $\lambda_i - \Delta\lambda$ and λ_i. The constant k_1 and k_2 can be inferred from equation (10). All the images are scaled to wavelength λ_i for the subtraction. Equation (12) is called fifth-order SSA or simply high-order SSA, and it is based on the third-order SSA subtraction.

3.3. *SSA Simulations*

As discussed by Racine et al. (1999), subtracting simultaneous images can defeat speckle noise. In the simulations, the wave-front error is created randomly by using 24 term Zernike polynomials, in which the tip/tilt components are removed to avoid possible centering error. This represents a low-frequency wave-front error on the pupil. The low-frequency wave-front error that results in speckle noise close to the PSF center represents a worse case for the local contrast than high-frequency. The spectral resolution is chosen to be 100, since *TPF-C* will probably provide such a resolving power for spectroscopy in the visible. Based on experience with the *Hubble Space Telescope*, we assume that a Strehl ratio will not be better than 0.90. The Strehl ratio is chosen between 0.70 and 0.90. The PSF peak intensity is normalized to unity. To explore the speckle noise, the aberrated PSF of the starlight is subtracted by a reconstructed perfect PSF so that only wave-front-induced speckle noise is left.

Figure 1 is the result of the low-order SSA at 0.90 Strehl ratio. The rms (root mean square) aberrated PSF (*dotted line*) and the speckle noise (*dash-dotted line*) at $4\lambda/D$ is 1.4×10^{-3} and 6.1×10^{-4}, respectively. After low-order SSA subtractions, the rms residual speckle noises is 2.7×10^{-6} (third-order SSA, *solid line*) and 1.1×10^{-5} (second-order SSA, *dashed line*), respectively. Contrast gains of $\sim 10^{-2}$ are achieved; the low-order SSA subtractions at 0.80 Strehl ratio are presented in Figure 2. A summary of the low-order SSA at $4\lambda/D$ at different Strehl ratios is listed in Table 1.

The amazing gains of the high-order SSA subtractions are demonstrated in Figure 3 with 0.90 Strehl ratio. After high-order SSA subtractions, the rms residual speckle noise at $4\lambda/D$ is 1.9×10^{-8} (fifth-order SSA, *solid line*) and 5.3×10^{-8} (fourth-order SSA, *dashed line*), respectively. Contrast gains of $\sim 10^{-5}$ are achieved. The powerful attenuation of the high-order SSA subtraction means that it can tolerate large wave-front error; the high-order SSA subtractions at 0.80 Strehl ratio are presented in Figure 4. A summary of the high-order SSA at $4\lambda/D$ at different Strehl ratios is listed in Table 2.

It is clear that both low-order and high-order SSAs can provide a stable speckle subtraction at different Strehl ratios. For low-order SSAs the third-order SSA is superior to the second-order SSA, while for the high-order SSAs the fifth-order SSA is superior to the fourth-order SSA. This is consistent with our previous theoretical calculations that a high-order SSA has a high-order residual speckle term that dominates the residual speckle noise.

Figure 5 is the simulation for the star and planet imaging at 0.90 Strehl ratio. The planet is located $4\lambda/D$ away from the star and with an intensity of only 10^{-7} that of the star. The left panel (intensity in logarithmic scale) is the image of the aberrated star PSF, while the central panel (intensity in linear scale) is the star speckle noise after the perfect PSF is removed. The central panel is overexposed to shown the faint structure of the speckle noise. The speckle noise shows strong asymmetry since it is dominated by the first-order speckle noise $I_{\rm odd1}$, which has negative and positive values in the PSF focal plane. In both panels, the planet image is included but of course is not visible. The final image after the subtraction of the fifth-order SSA is shown in the right panel (intensity in linear scale). After SSA subtraction, the planet images are clearly visible with a S/N $\sim$ 10. Residual high-order speckles are still visible close to the PSF even after SSA subtraction.

Although we only demonstrated SSA subtractions at 100 spectral resolution, the contrast gains could be scaled to other resolving powers. For the low-order SSA subtraction, the dominant residual speckle noise is inversely proportional to the spectral resolution; since the low-order SSA is performed twice, the dominant residual noise for the high-order SSA is inversely

TABLE 1
SUMMARY OF THE LOW-ORDER SSA SUBTRACTIONS AT $4\lambda/D$

	SECOND-ORDER SSA			THIRD-ORDER SSA		
STREHL RATIO	0.70	0.80	0.90	0.70	0.80	0.90
Aberrated PSF	2.7×10^{-3}	1.9×10^{-3}	1.4×10^{-3}	2.7×10^{-3}	1.9×10^{-3}	1.4×10^{-3}
Speckle noise	2.1×10^{-3}	1.3×10^{-3}	6.1×10^{-4}	2.1×10^{-3}	1.3×10^{-3}	6.1×10^{-4}
Residual speckle noise	1.1×10^{-4}	4.3×10^{-5}	1.1×10^{-5}	1.6×10^{-5}	6.2×10^{-6}	2.7×10^{-6}
Contrast gain	5.2×10^{-2}	3.3×10^{-2}	1.8×10^{-2}	7.6×10^{-3}	4.8×10^{-3}	4.4×10^{-3}

proportional to the square of the spectral resolution. For the same Strehl ratio, the contrast gain at 100 spectral resolution is 100 times better than that at 10 spectral resolution for the high-order SSA.

Both the low- and high-order SSAs result in two duplication companion images, since they are based on the direct subtraction discussed in § 2.1. This is not a problem for the imaging of the point-source companion in most cases. In fact, the duplication of the companion's image can be avoided by applying the equation $\Delta\Delta I_i = [I_i(\lambda_i + \Delta\lambda) - k_1 I_i(\lambda_i)] - kk[I_i(\lambda) - k_2 I_i(\lambda_i - \Delta\lambda)]$ directly to equation (3): by adjusting the three intensity scale factors k_1,k_2, and kk, each subtraction for the $[I_i(\lambda_i + \Delta\lambda) - k_1 I_i(\lambda_i)]$ and $[I_i(\lambda_i) - k_2 I_i(\lambda_i - \Delta\lambda)]$ can eliminate one of the same order speckle, so that the subtraction $\Delta\Delta I_i = [I_i(\lambda_i + \Delta\lambda) - k_1 I_i(\lambda_i)] - kk[I_i(\lambda) - k_2 I_i(\lambda_i - \Delta\lambda)]$ can eventually eliminate both first- and second-order speckles, leaving the residual speckle noise dominated by the third-order speckle. The performance of such a subtraction should be very close to the second-order SSA, since the residual noise is dominated by the third-order speckle for both of them.

3.4. *White-Light Image Reassembly*

Finally, the monochromatic images discussed previously could be co-added to form a white-light image over a wide wavelength range. From equations (9)–(12), the starlight speckles have been efficiently attenuated, leaving the planet's image after the subtractions at the planet absorption spectra. Since the subtractions are done at each of the absorption (or emission) wavelengths, this results in a three-dimensional data cube in which each of the monochromatic images is available. A white-light image I_P of the planet can be re-assembled from such a date cube. According to equations (9)–(12), the integration of wavelengths would result in a white-light image, which is expressed as

$$I_P = \sum_{i=1}^{n} \Delta I_i(\lambda_i) \tag{13}$$

or

$$I_P = \sum_{i=1}^{n} \Delta\Delta I_i(\lambda_i). \tag{14}$$

The wavelength integration to construct the white-light image provides a possibility for the "blind subtraction": that is, for the SSA subtractions, it is not necessary to know exactly the wavelength locations of the absorption (or emission) spectra. The spectral subtraction could be done continuously in wavelengths one by one until it covers the entire wavelength range. Since the scale factors are calculated according to the starlight, the continuum images of the starlight are always subtracted, while the planet differential images remain.

3.5. *Other Noises*

With the dominant speckles removed, other noises such as photon, field-flat, and read noises will become dominant. Racine

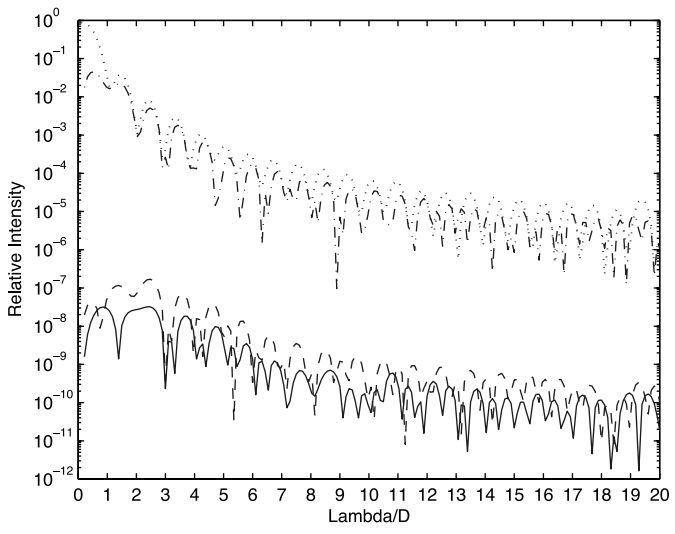

FIG. 3.—Contrast achieved with the high-order SSA at 0.90 Strehl ratio. Dotted line shows the aberrated PSF. Dash-dotted line shows the speckle noise after the perfect star PSF is removed. Solid and dashed lines represent the residual speckle noise after the fifth-order and fourth-order SSA subtractions, respectively. Contrast gain is typically $\sim 10^{-5}$. [*See the electronic edition of the Journal for a color version of this figure.*]

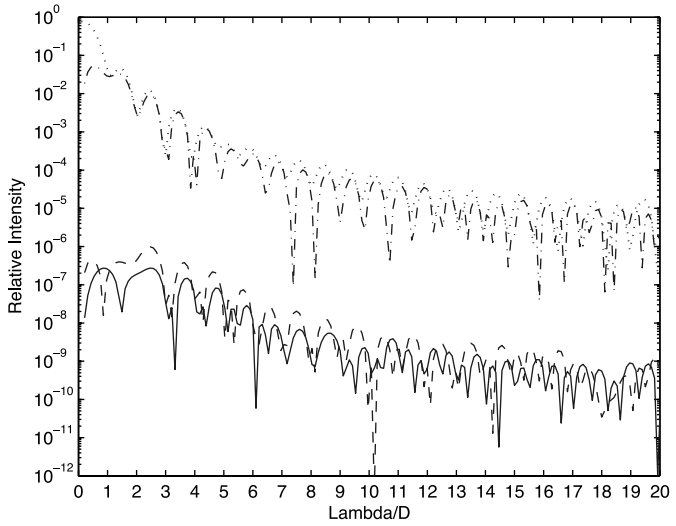

FIG. 4.—Same as Fig. 3, except that the Strehl ratio is 0.80. Contrast gain is typically $\sim 10^{-4}$. [*See the electronic edition of the Journal for a color version of this figure.*]

TABLE 2
SUMMARY OF THE HIGH-ORDER SSA SUBTRACTIONS AT $4\lambda/D$

	FOURTH-ORDER SSA			FIFTH-ORDER SSA		
STREHL RATIO	0.70	0.80	0.90	0.70	0.80	0.90
Aberrated PSF	2.7×10^{-3}	1.9×10^{-3}	1.4×10^{-3}	2.7×10^{-3}	1.9×10^{-3}	1.4×10^{-3}
Speckle noise	2.1×10^{-3}	1.3×10^{-3}	6.1×10^{-4}	2.1×10^{-3}	1.3×10^{-3}	6.1×10^{-4}
Residual speckle noise	6.5×10^{-7}	2.7×10^{-7}	5.3×10^{-8}	5.2×10^{-7}	1.5×10^{-7}	1.9×10^{-8}
Contrast gain	3.1×10^{-4}	2.1×10^{-4}	8.7×10^{-5}	2.5×10^{-4}	1.2×10^{-4}	3.1×10^{-5}

et al. (1999) presented a detailed discussion, which gave quantitative calculations. Here we not present such a quantitative analysis. Instead, we do provide a brief discussion about possible strategies to ensure that we can benefit mostly from the results of the SSA subtractions.

Nakajima (1994) discussed the possibility of planet detection with ground-based adaptive optics. He only considered the photon noise, and concluded that such a detection is feasible for a ground-based telescope with 6.5 m aperture. Although it is too optimistic, since other noises may limit the performance, it is valid if only photon noise exists. In such a situation, the S/N could be further increased by having better image quality (higher Strehl ratio) and longer exposure time (or a larger aperture telescope for ground observing); sky background random noise is also time-dependent. This means that increasing the overall exposure time could improve the S/N, if the quasi-component could be efficiently subtracted.

Detector read noise also needs to be considered. Repeatedly reading out the signal could increase the S/N, since the random read noise increases as the square root of the read-out number, while the signal increases linearly. Such a strategy was discussed by Fowler & Gatley (1990) for the infrared imaging where the read-out is the dominant source of noise. Currently, "zero-read noise" photon counting detectors (Graham et al. 2004; Basden et al. 2003) are being developed for the direct detection of extrasolar planets. Furthermore, since the read noise is independent of the exposure time, increasing the overall exposure time could efficiently increase the S/N.

To match the high-order SSA, flat-fielding with 10^{-4} to 10^{-5} accuracy is required. Flat-field accuracy $\sim 10^{-3}$ was reported (Tyson 1986). It seems that the actual accuracy is limited by the illumination uniformity for the flat-field calibration. Accuracy better than 10^{-4} was demonstrated by numerical simulation (Kuhn et al. 1991).

Finally, geometrical image distortion may be a concern for the SSA subtraction since it involves a wavelength scaling. As we see in next section, the requirement for the centering accuracy is the order of 1 pixel if λ/D is sampled by 8 pixels. This is also applied to the image distortion, and this results a requirement of $\sim$1/500 overall accuracy for the filed distortion if a 1k $\times$ 1k detector array is used. This is a strict requirement that ensures that the position displacement is always less than 1 pixel even at the edge of the array. However, such a displacement is a function of the distance to the star. At the star intensity peak, which is defined as the original for the scaling, there is no displacement no matter how large the distortion. The displacement is gradually increased until it reaches 1 pixel at the array edge; for a small interesting area, if only $10\lambda/D$ radius is considered and it is sampled by 200×200 pixel detector array. The 1 pixel accuracy results a requirement of 1/100 field distortion. Present-day optical system can achieve $\sim$2% distortion. Depending on the application, it is expected that some calibration may be needed to further correct the distortion.

4. CENTERING SENSITIVITY

One of the possible error sources for the SSA subtraction is the PSF centering. The centering error may be introduced in the process of the image rotation, so that the two images could not be registered correctly for the direct subtraction.

The Zernike polynomials may introduce a position registration error since we only simply remove the tip/tilt term while other Zernike terms may also introduce a PSF position shift. In the simulations in the above examples, the pupil is sampled by 100×100 pixels. At the focal plane the PSF is sampled by

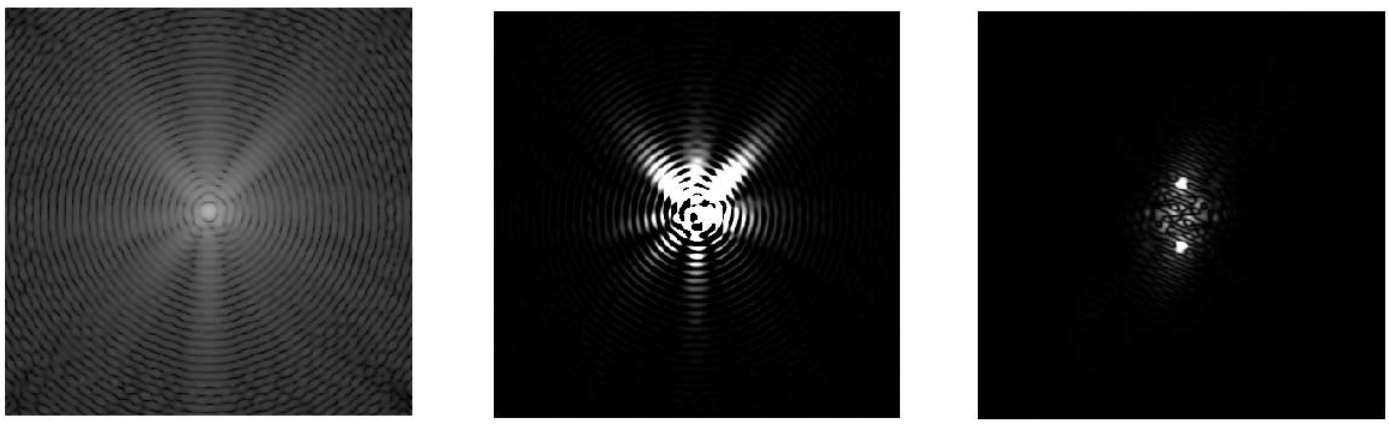

FIG. 5.—Raw image of the star and a companion (*left panel*) at 0.90 Strehl ratio. The planet peak intensity is only 10^{-7} that of the star. The aberrated PSF of the star image clearly shows asymmetry because of the wave-front error. The speckle noise after the perfect star PSF is removed is shown in the center panel, in which the companion is buried in the noise and is not visible. Right panel is the image after the fifth-order SSA subtraction, and the companion's images are now clearly visible with a S/N $\sim$ 10.

800×800 pixels, while the λ/D is sampled by 8 pixels. This corresponds to a (100×100) λ/D field of view. The sampling accuracy is better than one pixel and it is determined by the number of pixels used to sample the PSF. This implies if the PSF of the same field is sampled by a larger detector array such as an $1k \times 1k$ array, the centering accuracy could be better than that of the 800×800 pixels in the simulation.

For all the examples, bright PSF disks with a circular aperture without focal plane obscuration are used for the centering. For coronagraph with focal plane obscuration, PSF centering could be done by using the diffraction pattern at a monochromatic images. Post–data reduction, automatically searching for the best centering position is possible by using the starlight intensity as a merit function, since at the best position the residual speckle noise at the interesting region should be minimized.

5. CONCLUSIONS

The fact that the aberrated PSF could be expressed via a Taylor series provides an opportunity to remove the low-order as well as the high-order speckles. We propose an algorithm that consists of a low-order as well as a high-order SSAs. The performance of the SSA is a function of the spectral resolution and the wave-front error. For the low-order SSA, it can remove up to the third-order speckle noise, and the performance is inversely proportional to the spectral resolution. At the 0.90 Strehl ratio and 100 spectral resolution, the low-order SSA subtraction can provide an extra contrast gain of $\sim 10^{-2}$; for the high-order SSA, it can remove up to the fifth-order speckle noise and can further improve the contrast performance, which is inversely proportional to the square of spectral resolution. At 0.7–0.90 Strehl ratio and 100 spectral resolution, it can provide an amazing contrast gain of 10^{-4} to 10^{-5}. To our knowledge, this is the first demonstration that such high-order speckles can been removed.

Combined with a coronagraph, such SSA subtractions can significantly improve the performance that would otherwise be degraded by the wave-front error, and greatly relax the requirement for the wave-front quality for both the exoplanet imaging and the biomarker spectroscopy. For a space mission, no AO correction is required, as we have demonstrated that the SSA subtractions can provide a significant contrast gain at Strehl ratio 0.70–0.90.

Although the SSA subtractions discussed here are aimed for a space mission, such an approach also has the potential for ground-based high-contrast imaging if a moderately high AO correction (with Strehl ratio 0.70–0.80) is available and the centering can be done accurately. In such an application, an ultrafast (faster than the speckle dwell time) and ultrastable tip/tilt mirror is required so that the centering accuracy is not a problem. Series of subexposures, each with a short exposure, could be taken and then co-added, as done in the same way for the space system. In this process, bad data of the subexposures could be rejected in the data reduction process, which would enhance the success for the high-contrast imaging.

We acknowledge that the scintillation is also important for the high-contrast imaging; however, it is beyond the scope of this paper. Detailed simulations using biomarker spectra including scintillation will be discussed in future papers.

The authors thank A. Sivaramakrishnan and E. Bloemhof for invaluable discussions. We are grateful to the referee, R. Racine, who has provided very detailed and helpful comments that significantly improved the paper. This work is supported by National Science Foundation under the grant AST 05-01743.

REFERENCES

Aime, C., & Soummer, R. 2004, ApJ, 612, L85
Basden, A. G., Haniff, C. A., & Mackay, C. D. 2003, MNRAS, 345, 985
Baudoz, P., Rabbia, Y., & Gay, J. 2000, A&AS, 141, 319
Bloemhof, E. E. 2003, ApJ, 582, L59
———. 2004a, Opt. Lett., 29, 2333
———. 2004b, ApJ, 610, L69
Bloemhof, E. E., & Oppenheimer, B. R. 2001, ApJ, 558, L71
Boccatletti, A, Riaud, P., & Rouan, D. 2002, PASP, 114, 132
Bracewell, R. N. 1986, The Fourier Transform and its Applications (2nd ed.; New York: McGraw-Hill)
Butler, R. P., et al. 2003, ApJ, 582, 455
Fowler, A. M., & Gatley, I. 1990, ApJ, 353, L33
Gonsalves, R., & Nisenson, P. 2003, PASP, 115, 706
Graham, M. C., Potter, D. E., & Close, L. 2004, Proc. SPIE, 5492, 545
Guyon, O., Pluzhnik, E. A., Galicher, R., Martinache, F., Ridgway, S. T., & Woodruff, R. A. 2005, ApJ, 622, 744
Kasdin, N. J., Vanderbei, R. J., Littman, M. G., Ren, D., Carr, M., & Spergel, D. N. 2004, BAAS, 205, 514
Kasdin, N. J., Vanderbei, B. J., Spergel, D. N., & Littman, M. G. 2003, ApJ, 582, 1147
Kuchner, M. J., & Traub, W. A. 2002, ApJ, 570, 900
Kuhn, J. R., Lin, H., & Loranz, D. 1991, PASP, 103, 1097
Marcy, G. W., et al. 2002, ApJ, 581, 1375
Marois, C. Doyon, R., Racine, R., & Nadeau, D. 2000, PASP, 112, 91
Nakajima, T. 1994, ApJ, 425, 348
Nisenson, P., & Papaliolios, C. 2001, ApJ, 548, L201
Perrin, M. D., Sivaramakrishnan, A., Makidon, R. B., Oppenheimer, B. R., & Graham, J. R. 2003, ApJ, 596, 702
Racine, R. Walker, G. A. H., Nadeau, D., Doyon, R., & Marois, C. 1999, PASP, 111, 587
Ren, D., & Allington-Smith, J. R. 2002, PASP, 114, 866
Ren, D., & Ge, J. 2004, PASP, 116, 46
Ren, D., & Serabyn, E. 2005, Appl. Opt., 44, 7070
Rosenthal, E. D., Gurwell, M. A., & Ho, P. T. P. 1996, Nature, 384, 243
Rouan, D., Riaud, P., Boccaletti, A., Clénet, Y., & Labeyrie, A. 2000, PASP, 112, 1479
Sivaramakrishnan, A., Koresko, C. D., Makidon, R. B., Berkefeld, T., & Kuchner, M. J. 2001, ApJ, 552, 397
Sivaramakrishnan, A., Lloyd, J. P., Hodge, P. E., & Macintosh, B. A. 2002, ApJ, 581, L59
Sparks, W. B., & Ford, H. C. 2002, ApJ, 578, 543
Tinney, C. G., et al. 2003, ApJ, 587, 423
Tyson, J. A. 1986, J. Opt. Soc. Am. A, 3, 2131
Vanderbei, R. J., & Traub, W. A. 2005, ApJ, 626, 1079